

Predicting Relapse in Patients With Medulloblastoma by Integrating Evidence From Clinical and Genomic Features

Pablo Tamayo, Yoon-Jae Cho, Aviad Tsherniak, Heidi Greulich, Lauren Ambrogio, Netteke Schouten-van Meeteren, Tianni Zhou, Allen Buxton, Marcel Kool, Matthew Meyerson, Scott L. Pomeroy, and Jill P. Mesirov

See accompanying editorial on page 1395 and articles on pages 1400, 1408, and 1424

From the Eli and Edythe Broad Institute of Massachusetts Institute of Technology and Harvard University, Cambridge; Dana-Farber Cancer Institute; Brigham and Women's Hospital, Harvard Medical School; Children's Hospital, Boston, MA; Academic Medical Center, Amsterdam, the Netherlands; and Children's Oncology Group, Arcadia, CA.

Submitted January 15, 2010; accepted December 13, 2010; published online ahead of print at www.jco.org on February 28, 2011.

Supported by Grants No.

R01-CA109467, R01-CA105607, R01-CA121941, R01-GM074024, P50-CA112962, and P30-HD018655.

S.L.P. and J.P.M. contributed equally to this work.

Authors' disclosures of potential conflicts of interest and author contributions are found at the end of this article.

Clinical Trials repository link available on JCO.org.

Corresponding author: Jill P. Mesirov, PhD, Broad Institute of MIT and Harvard, 7 Cambridge Center, Cambridge, MA 02142; e-mail: mesirov@broad.mit.edu.

© 2011 by American Society of Clinical Oncology

0732-183X/11/2911-1415/\$20.00

DOI: 10.1200/JCO.2010.28.1675

A B S T R A C T

Purpose

Despite significant progress in the molecular understanding of medulloblastoma, stratification of risk in patients remains a challenge. Focus has shifted from clinical parameters to molecular markers, such as expression of specific genes and selected genomic abnormalities, to improve accuracy of treatment outcome prediction. Here, we show how integration of high-level clinical and genomic features or risk factors, including disease subtype, can yield more comprehensive, accurate, and biologically interpretable prediction models for relapse versus no-relapse classification. We also introduce a novel Bayesian nomogram indicating the amount of evidence that each feature contributes on a patient-by-patient basis.

Patients and Methods

A Bayesian cumulative log-odds model of outcome was developed from a training cohort of 96 children treated for medulloblastoma, starting with the evidence provided by clinical features of metastasis and histology (model A) and incrementally adding the evidence from gene-expression–derived features representing disease subtype–independent (model B) and disease subtype–dependent (model C) pathways, and finally high-level copy-number genomic abnormalities (model D). The models were validated on an independent test cohort ($n = 78$).

Results

On an independent multi-institutional test data set, models A to D attain an area under receiver operating characteristic (au-ROC) curve of 0.73 (95% CI, 0.60 to 0.84), 0.75 (95% CI, 0.64 to 0.86), 0.80 (95% CI, 0.70 to 0.90), and 0.78 (95% CI, 0.68 to 0.88), respectively, for predicting relapse versus no relapse.

Conclusion

The proposed models C and D outperform the current clinical classification schema (au-ROC, 0.68), our previously published eight-gene outcome signature (au-ROC, 0.71), and several new schemas recently proposed in the literature for medulloblastoma risk stratification.

J Clin Oncol 29:1415-1423. © 2011 by American Society of Clinical Oncology

INTRODUCTION

Medulloblastomas are primitive embryonal tumors of the CNS arising in the cerebellum and disseminating throughout the CNS. Over the past 15 years, significant progress has been made in understanding the biologic mechanisms driving these tumors.¹ These advances provide a growing framework for new risk stratification schemas and targeted therapies. Efforts to determine risk in the context of current treatment seek to improve overall survival and decrease long-term deficits associated with multimodal treatment regimens

based on conventional chemotherapy, surgical resection, and craniospinal irradiation.²⁻⁵

The current clinical medulloblastoma classification schema, based on age and metastasis status at diagnosis, extent of initial resection, and histology, has limited predictive power. However, 5-year survival rates for standard-risk patients can be up to 85%, with 60% to 80% for high-risk groups. Despite this relative success, survival almost universally comes at the expense of long-term neurologic and neurocognitive deficits resulting from the aggressiveness of the treatments. Importantly, the current clinical schema fails to identify a significant group of

Table 1. Features or Risk Factors Used by the Bayesian Cumulative Log-Odds Model to Predict Relapse

Feature	Values	Patients (%)	Posterior Log-Odds Ratio Ev (r x; 95% CI)						Average Absolute Evidence (Avev)	Description	Source	Gene Set Reference
			c1	c2	c3	c4	c5	c6				
Relapse (prior)			-0.28						0.28	Prior		
Clinical												
Histology	Classic	68	0.0033 ± 0.06						0.094	Tumor histology at diagnosis		
		Desmo	14	-0.34 ± 0.20								
	LCA	17	0.27 ± 0.02									
Metastasis	Yes M1-4	17	0.58 ± 0.07						0.236	Metastasis status at diagnosis		
	No M0	75	-0.16 ± 0.18									
Subtype-independent expression signature												
c-Myc activation	High	44	0.53 ± 0.22						0.485	Genes upregulated (43) and downregulated (65) by c-Myc	MSigDB v2.5/C2	YU_CMYC_UP/DN Yu et al ³⁴
	Low	56	-0.45 ± 0.25									
Disease subtype (c1-c6)												
c1	c1	15	0.69 ± 0.03						0.352	Disease subtype as determined by gene expression See Appendix		
		c2	18	-0.25 ± 0.13								
		c3	29	0.23 ± 0.23								
		c4	19	-0.33 ± 0.16								
		c5	9.4	0.08 ± 0.22								
		c6	10	-0.68 ± 0.52								
DNA copy number gains or losses												
amp(8q24.21)	Amp	3.1	0.44 ± 0.40						0.113	Amplification of chr8q24.21. Locus of c-Myc ¹⁴		
	(c-MYC)	Norm	36	-0.085 ± 0.83								
amp(2p24.3)	Amp	15	0.50 ± 0.36						0.421	Deletion of chr6q. Monosomy 6 ¹⁴		
	(N-MYC)	Norm	25	-0.37 ± 1.53								
del(6q) (monosomy 6)	Del	6.2	-0.12 ± 0.88						0.047	Deletion of chr16q		
	Norm	33	0.033 ± 0.68									
del(16q)	Del	15	0.95 ± 0.24						0.855	Deletion of chr16q23.3		
	Norm	25	-0.80 ± 3.8									
del(16q23.3)	Del	16	0.83 ± 0.26						0.786	Amplification of chr7q21.3		
	Norm	24	-0.76 ± 3.84									
amp(7q21.3)	Amp	15	0.73 ± 0.22						0.63	Amplification of chrq26.32. Locus of p110a/PI3K		
	Norm	25	-0.57 ± 4.03									
amp(3q26.32)	Amp	8.3	1.1 ± 0.25						0.581			
	Norm	0.31	-0.45 ± 2.05									
Subtype-dependent expression signatures												
mTOR induced	High	42	0.44 ± 0.11	0.81 ± 0.22	0.20 ± 0.18	0.47 ± 0.22	-0.11 ± 0.03	0.69 ± 0.22	0.382	Genes upregulated (200) and downregulated (200) by mTOR	OPAM v3	mTOR_UP.v1 Majumder et al ³⁵
	Low	58	0.59 ± 0.22	-0.61 ± 0.59	-0.25 ± 0.03	-0.22 ± 0.23	0.12 ± 0.23	-0.22 ± 0.38				
Anti-CD44 regulated	High	57	-0.37 ± 0.22	-0.05 ± 0.16	0.00 ± 0.22	-0.22 ± 0.23	-0.98 ± 1.12	-0.12 ± 0.29	0.22	Genes upregulated (20) and downregulated (7) by c-MYC	MSigDB v2.5/C2	HOGERKORP_CD44_UP; Högerkorp et al ³⁶
	Low	43	0.14 ± 0.09	0.12 ± 0.06	0.00 ± 0.22	0.47 ± 0.22	0.81 ± 0.05	0.29 ± 0.10				
c-MYC activated (v2)	High	43	0.10 ± 0.08	-0.11 ± 0.14	1.20 ± 0.10	-0.22 ± 0.23	-0.39 ± 0.18	0.69 ± 0.19	0.441	Histidine metabolism genes (25)	MSigDB v2.5/C2	Coller et al ³⁷

(continued on following page)

Table 1. Features or Risk Factors Used by the Bayesian Cumulative Log-Odds Model to Predict Relapse (continued)

		c ₁	c ₂	c ₃	c ₄	c ₅	c ₆					
	Low	57	-0.14 ± 0.23	0.05 ± 0.06	-0.63 ± 0.27	0.29 ± 0.03	0.34 ± 0.22	-0.69 ± 1.41		Genes (30) downregulated by Gli1	OPAM v3	HISTIDINE_METABOLISM
Histidine metabolism	High	56	1.3 ± 1.00	-0.15 ± 0.13	0.00 ± 0.22	0.47 ± 0.22	0.12 ± 0.18	0.29 ± 0.10	0.341			KEGG pathway ³⁸
	Low	44	0.64 ± 0.11	-0.12 ± 0.06	0.00 ± 0.22	-0.92 ± 1.88	-0.11 ± 0.03	-0.41 ± 0.58		Ribavirin/RSV-induced upregulated (22) and downregulated (43) response	MSigDB v2.5/C2	GLI1_UP.v1_DN
Gli1 downregulated	High	57	0.08 ± 0.04	0.54 ± 0.18	0.00 ± 0.22	0.11 ± 0.08	-0.44 ± 0.21	-0.22 ± 0.38	0.275			Yoon et al. ³⁹
	Low	43	0.14 ± 0.08	-0.98 ± 2.22	0.00 ± 0.22	-0.22 ± 0.23	0.81 ± 0.05	0.69 ± 0.19				RIBAVIRIN_RSV_UP(DN)
Ribavirin/RSV-induced response	High	56	0.23 ± 0.23	0.22 ± 0.02	0.00 ± 0.22	-0.54 ± 0.56	-0.17 ± 0.06	0.29 ± 0.11	0.25			Zhang et al. ⁴⁰
	Low	44	0.55 ± 0.12	-0.18 ± 0.18	0.00 ± 0.22	0.65 ± 0.18	0.12 ± 0.18	-0.41 ± 0.58				

Abbreviations: Desmo, desmoplastic; LCA, large-cell/anaplastic; MSigDB, Molecular Signatures Database; Amp, amplified; Norm, normal; Del, deletion; RSV, respiratory syncytial virus.

patients (approximately 20%) who are categorized as standard-risk but do not respond to treatment. Because of these limitations, the search for better risk stratification schemas based on molecular markers and genomic abnormalities have become the focus of interest in the last decade.^{6,7}

Histology has been associated with clinical outcome⁸⁻¹⁰; however, because tumors display highly variable degrees of heterogeneity, subtyping via traditional histopathology is especially difficult. Several molecular markers and genomic abnormalities have been shown to correlate with poor clinical outcome, including *c-Myc* amplification,¹¹ 17p loss/i(17)q,¹² concomitant expression of *LDHB/CCNB1*,¹³ gain of 6q/17q,¹⁴ and overexpression of *CDK6*¹⁵ and survivin.¹⁶ Similarly, β -catenin mutations and monosomy 6^{17,18} and overexpression of *TrkC*¹⁹ have been associated with good clinical outcome. However, statistical association with clinical outcome does not necessarily yield accurate classification on a case-by-case basis. In addition, many of these genomic markers suffer from low penetrance and modest sensitivity/specificity. Thus, they are rather limited as prognostic markers alone and are not routinely used in the clinic to evaluate risk.

We previously introduced an eight-gene molecular signature⁶ that was effective at separating patients in standard-risk and high-risk groups (80% v 17% 5-year overall survival, respectively) and outperformed the current clinical schema but was less accurate for data sets beyond the original study (Data Supplement). Moreover, while we observed a number of molecular subtypes of medulloblastoma in that study, we had insufficient numbers of samples to assess whether outcome signatures varied by subtype.

In the ensuing years, there have been a number of advances in molecular signature analysis. In our own work, we established the increased strength of using sets of genes rather than individual genes to distinguish biologic phenotypes.^{20,21} We extended this method to evaluate the activity of a set of genes in a single sample and used it effectively in two recent studies.^{22,23} Other signature approaches were also introduced.²⁴⁻²⁶ More recently, methods integrating clinical data and genomic features^{13,14} have been applied to a variety of clinical prediction problems.²⁷⁻³¹

Here, we describe a novel method for predicting response to therapy (relapse/no relapse) for medulloblastoma and establish its efficacy on independent test data. We combine clinical data with molecular subtypes, pathway activation signatures, and copy number

data. Importantly, our method goes beyond establishing association with these risk factors and instead gives a predictive probability of relapse within 30 months of treatment. The method is based on a Bayesian cumulative log-odds model that computes the total evidence for relapse in each patient from the status of clinical and genomic features. This approach is general and provides a paradigm for genomic-based clinical prediction applicable to other tumor types. We also introduce a novel Bayesian nomogram³² for assessing a patient's overall risk on the basis of the positive/negative contribution of individual risk factors (the model features).

With better classification performance than the current clinical schema in use by the Children's Oncology Group (COG) and other cooperatives, the approach presented here shows promise to improve risk stratification for standard therapeutic protocols. The deployment of our model will require expression array and single nucleotide polymorphism–array profiling of each tumor, or alternatively, the development of clinical assays for rapid evaluation of expression and copy-number alteration in a few hundred genes. The subtypes identified in this model could also be relevant to future therapeutic strategies that directly target the molecular mechanisms of tumorigenesis.

PATIENTS AND METHODS

Patients

Tumor samples were obtained through the COG Tumor Bank (protocol ACNS02B3) and from Children's Hospital Boston, University of Washington Medical Center, Texas Children's Hospital, and The Johns Hopkins University Medical Center under approval from the respective institutional review boards. The training set consisted of 96 samples for which relapse status at 30 months post-treatment was known. Matched normal blood samples were collected through the COG Tumor Bank (protocol ACNS02B3) and from Children's Hospital Boston under institutional review board approval. The test set included 78 samples: 47 samples from our original study⁶ not used for training, 16 samples from Kool et al.,³³ and 15 samples from the COG Tumor Bank. All training and test samples correspond to patients at least 3 years old treated with conventional chemotherapy, surgical resection, and craniospinal irradiation (Table 1; Data Supplement). For all samples, we generated gene-expression and copy-number data using Affymetrix HT-HG-U133A2 and Affymetrix 250k and 6.0 arrays (Affymetrix, Santa Clara, CA), respectively

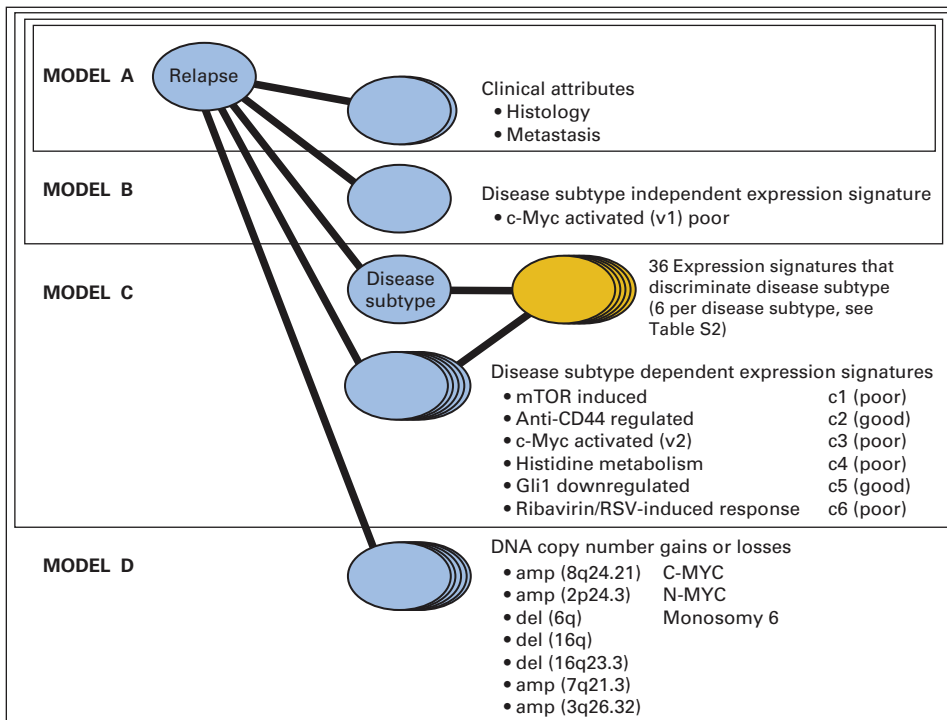


Fig 1. Bayesian cumulative log-odds model (probabilistic network) that integrates clinical and high-level genomic information to predict the probability of relapse. The submodel of model C corresponding to subtype determination is shown in a different color because it is applied separately and in advance for any unlabeled sample. RSV, respiratory syncytial virus.

(see Appendix), and we assigned risk categories according to current clinical criteria.^{2,7}

Determining Molecular Subtype

To predict the relapse status of a new sample (in the test set) its disease subtype (*c*) must first be determined. Six molecular subtypes {*c*₁, ... , *c*₆} of the samples in the training set were defined by clustering in a separate study (see Appendix) on a larger collection of about 200 medulloblastoma samples.⁴¹ These disease subtypes are linked to molecular mechanisms of tumorigenesis (see Appendix) and are consistent with the findings of several independent studies.^{17,33} We then used these labels to train a disease-subtype prediction model for new samples.

To build the subtype prediction model, we used a collection of 2,599 gene sets drawn from our Molecular Signatures Database (MSigDB)²¹ and manually curated gene sets derived from data in the Gene Expression Omnibus (GEO; see Appendix). We estimated the activation score (degree

of upregulation) of these sets in each training set sample by using a single-sample version of Gene Set Enrichment Analysis (ssGSEA).^{21,22} We dichotomized the activation scores as low or high (see Appendix). Using this gene set view of the data, for each disease subtype, we chose six expression signatures that best discriminate its previously assigned subtype label within the training set according to the area under receiver operating characteristic (au-ROC) curve (Data Supplement).

Bayesian Predictive Model

Our model predicts relapse status, *r* = {yes, no}, by accumulating the relevant log-odds evidence implied by the molecular subtype and the values of clinical and genomic features for a specific patient sample. We start from the prior, which can be thought of as the probability of relapse/no relapse based on the proportion of patients in the training set who relapse/do not relapse. Formally, we use the log-odds prior, *Ev(r)*. We then define four nested

Table 2. Summary of Performance for the Current Clinical Schema (and model C inside the standard and high-risk groups) and Our Bayesian Cumulative Log-Odds Models A to D

Model	Description	Training Set				Test Set				
		au-ROC Curve	<i>P</i>	Error Rate	KM <i>P</i>	au-ROC Curve	95% CI	<i>P</i>	Error Rate	KM <i>P</i>
S	Clinical schema	0.62	.075	0.368	.0012	0.68	0.55 to 0.79	.0044	0.288	.045
A	Clinical features (histology and metastasis)	0.58	.101	0.406	.0767	0.73	0.61 to 0.85	.000601	0.321	.186
B	A + disease subtype-independent pathway: <i>c-Myc</i>	0.66	.00321	0.365	.0254	0.75	0.64 to 0.85	.000177	0.346	.000441
C	B + disease subtype-dependent pathways	0.87	5.2×10^{-10}	0.219	7.62×10^{-9}	0.80	0.7 to 0.89	1.07×10^{-6}	0.256	1.96×10^{-8}
D	C + DNA copy number gains or losses	0.84	4.94×10^{-9}	0.281	5.61×10^{-6}	0.78	0.67 to 0.88	5.56×10^{-6}	0.256	2.14×10^{-8}
C	Inside standard-risk group	0.88	2.8×10^{-7}	0.207	.0047	0.72	0.56 to 0.87	.0066	0.255	7×10^{-4}
C	Inside high-risk group	0.95	2.9×10^{-6}	0.138	.00038	0.83	0.56 to 0.86	.0085	0.273	.0076

Abbreviations: au-ROC, area under the receiver operating characteristic curve; KM, Kaplan-Meier.

submodels (A to D; Fig 1 and Table 1). Each model incrementally incorporates additional evidence associated with relapse from a different type of genomic feature: model A adds clinical attributes, a_i , including histology (classic, desmoplastic, and large-cell/anaplastic) and metastasis status (M0 v M1-4). Model B adds disease subtype-independent gene-expression signatures, e_p , that is, those associated with relapse across all tumor samples without dividing the cohort into molecular subtypes. Model C adds disease subtype-dependent gene-expression signatures, se_p , that are specific to the sample's molecular subtype $\{c_1, \dots, c_6\}$. Model D adds disease subtype-independent DNA copy-number gains and losses (genomic abnormalities), g_i . This incremental approach allows us to compare what we gain in accuracy with each addition of new evidence.

Model Feature Selection

We chose model features in two ways: by their association with clinical outcome in past studies and by their strong correlation with the relapse/no relapse phenotype in the training data.

For gene-expression signatures, e_i and se_p , we used the 2,599 gene sets and the gene set view of the data as described above. We chose one disease subtype-

independent expression signature representing *c-Myc* activation³⁴ because *c-Myc* overexpression has been shown to be associated with poor outcome in medulloblastomas.⁴² In addition, we confirmed that the signature was in the top 20 pathway discriminators of relapse in the training set according to the au-ROC curve (Data Supplement). For the disease subtype-dependent expression signatures, we selected one of the top 20 discriminators of relapse inside each disease subtype within the training set according to the au-ROC curve (Data Supplement). In all these selections, we favored signatures with a clear biologic interpretation and/or those obtained from published activation and repression experiments.

For genomic abnormalities, we selected DNA copy number gains or losses by using single nucleotide polymorphism array data that we generated in our separate study⁴¹ (see Appendix) and from which we identified statistically significant focal amplifications and deletions using Genomic Identification of Significant Targets in Cancer (GISTIC).⁴³ We then selected loci in two ways: (1) high association with relapse in the training data set [del(16q), del(16q23.3), amp(7q21.3), and amp(3q26.32); see Appendix] and (2) association with outcome in past studies [amp(8q24.21/*c-Myc*),

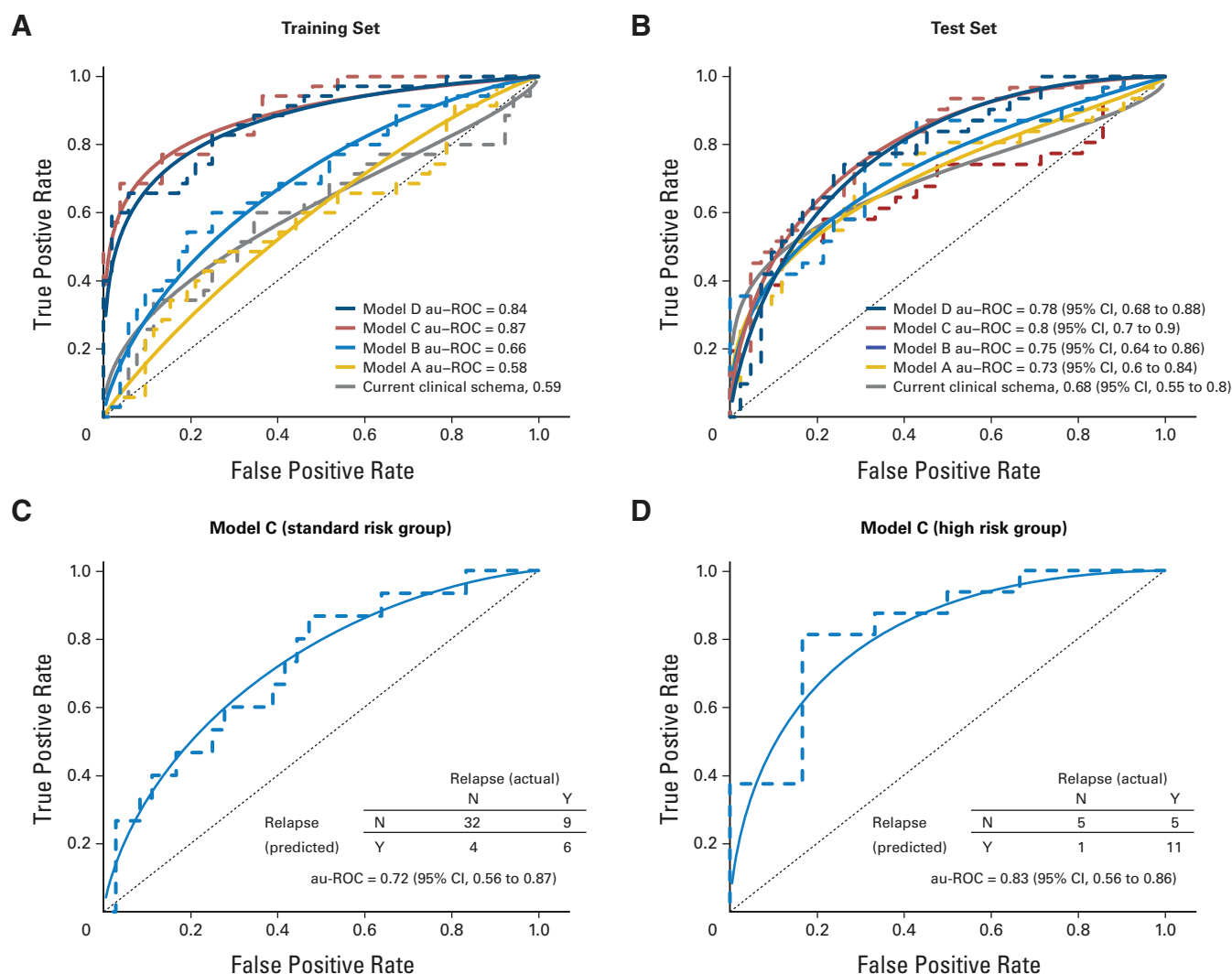


Fig 2. (A) Receiver operating characteristic (ROC) plots (empirical, dashed line; binormal, solid line) and area under the ROC (au-ROC) curve performance of the current clinical schema and models A to D in the training set. (B) ROC plot and au-ROC curve performance of the current clinical schema and models A to D in the independent test set. (C) ROC plots and au-ROC curve performance for model C in the independent test set for the standard-risk and (D) high-risk patient groups as defined by the current clinical schema. Note that only 73 of the test samples had corresponding clinical annotation that allowed categorization as standard risk or high risk. The model will still make a predictive call based on the genomic data. The 95% CIs in Figures 2B and 2C are estimates based on bootstrap sampling and are affected by small sample size. N, no; Y, yes.

amp(2p24.3/N-Myc) and del(6q/monosomy 6)]. Table 1 gives the log-odds association of each amplification or deletion with relapse. We used disease subtype-independent features because of the small number of samples with copy number data in the training set (38 of 96).

Training the Model

To set the parameters of the models, we evaluated the log-odds ratio, or conditional evidence, $Ev(r | x)$, for relapse, r , conditional on each feature x . We compute the contingency tables of feature versus relapse status in the training set where the value of r is known for each sample. This yields the probability of relapse of the training samples conditional on the value of that feature, $P(r | x)$, from which $Ev(r | x)$ can be computed (see Appendix).

Model Evaluation: Predicting Relapse

To predict relapse for a patient sample, we combine all of the evidence via a Bayesian cumulative log-odds model given by equation (1) with the value of each $Ev(r | x)$ determined by the value of each feature for the given sample.

$$Ev(r | \{x_i\}) = Ev(r) + \underbrace{\sum_{i=1}^{N_a} Ev(r | a_i)}_{\text{Model A: prior plus clinical attributes } a_i} + \underbrace{\sum_{i=1}^{N_e} Ev(r | e_i)}_{\text{Model B: A plus expression signatures } e_i} + Ev(r | c) + \underbrace{\sum_{i=1}^{N_{se,c}} Ev(r | se_{i,c}) + \sum_{i=1}^{N_g} Ev(r | g_i)}_{\text{Model C: B plus disease subtype } c \text{ and subtype-dependent expression signatures } se_i} + \underbrace{\hspace{10em}}_{\text{Model D: C plus genomic abnormalities } g_i} \tag{1}$$

To facilitate the interpretation of each prediction, we represent the individual log-odds evidence from each feature value graphically as arms in a Bayesian nomogram.³² Note that the nomogram is not the standard type used in regression models and that to predict the relapse status of a new (test) sample, its disease subtype c must first be determined separately as described above.

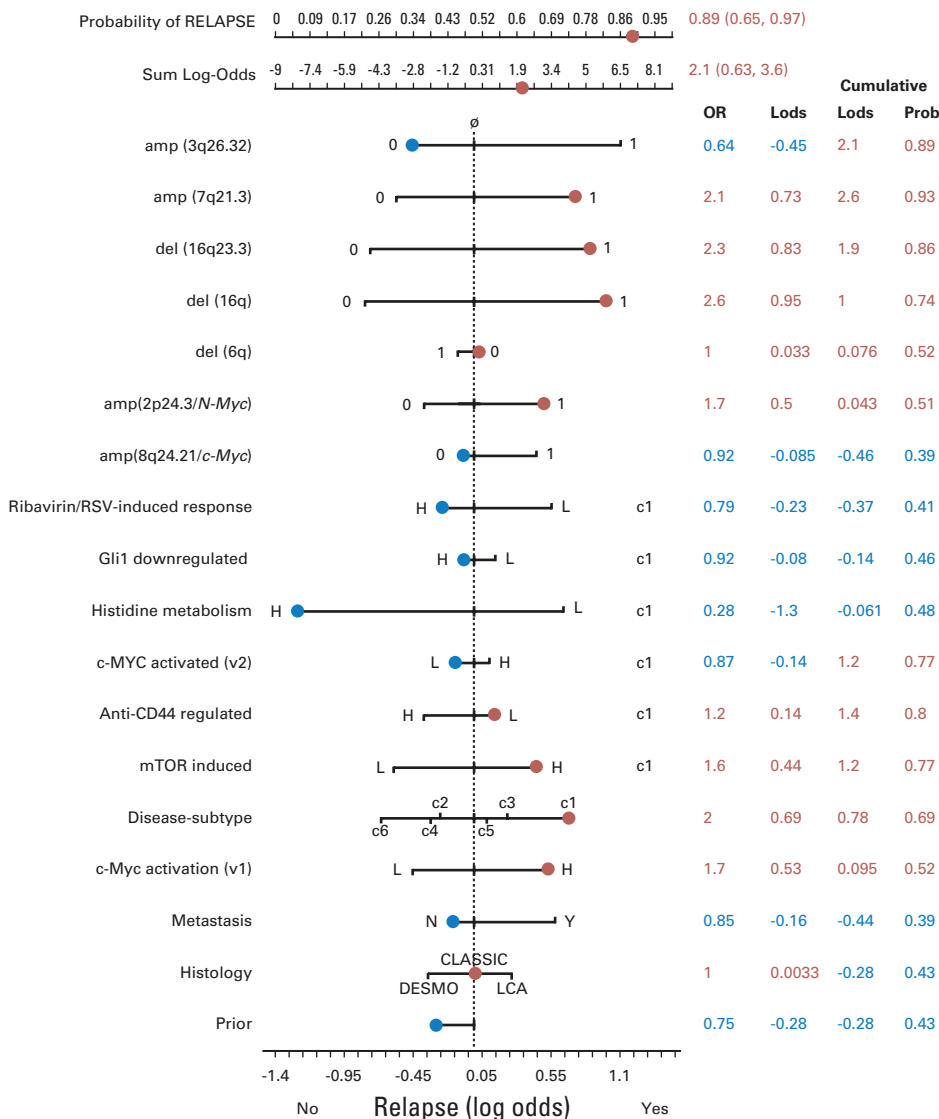


Fig 3. Bayesian nomogram showing the amount of evidence that each feature (risk factor) provides in the context of a specific patient's feature values. The arms of the nomogram represent the values of the posterior log odds ratio evidence, $Ev(r | x)$, for each feature's values. The actual values taken by each feature are shown in blue or red according to the sign of $Ev(r | x)$: positive magnitude to the right side is evidence for relapse (red) and negative magnitude to the left is evidence for no relapse (blue). The final sum of $Ev(r | x)$ provides the final probability of relapse, which is 0.89 (95% CI, 0.65 to 0.97). OR, odds ratio; Lods, log-odds; Prob, probability; RSV, respiratory syncytial virus; H, high; L, low; DESMO, desmoplastic; LCA, large-cell/anaplastic (lymphoma); N, no; Y, yes.

RESULTS

To validate models A to D, we assessed how well each model recapitulated the relapse end points of the 96 training samples. Next we used the independent set of 78 test patient samples to evaluate how well each model generalized to new data and how well it predicted patient relapse. To make a predictive call, we estimated the probability of relapse using the feature values of each patient sample in equation (1).

Model Fit on Training Data

Training performance improves as the models incorporate more feature types (Table 2, Fig 2A; Data Supplement). For example, the au-ROC curve values for models A to D are 0.58, 0.66, 0.87, and 0.84, respectively. The differences between models C and D are small, presumably because of the limited number of samples with known genomic abnormality status (see Discussion).

Performance on Test Data Sets

On the independent test set of 78 samples, the performance of models A to C increases overall (Table 2, Fig 2B) as more information is made available, with a small decrease in model D (see Discussion), demonstrating the benefits of cumulative integration of several sources of information including disease subtypes. For example, the au-ROC curve values for models A to D in the test set are 0.73, 0.75, 0.80, and 0.78, respectively. The corresponding Kaplan-Meier log-rank *P* values show a similar trend (Data Supplement) as do the relative utility curves⁴⁴ (Appendix and Data Supplement). Models C and D outperform the current clinical schema (au-ROC curve, 0.68; Fig 2B and Data Supplement), model A on the basis of clinical features alone (au-ROC curve, 0.73; Fig 2B and Data Supplement), and our previously published eight-gene outcome signature (au-ROC curve, 0.71; Data Supplement). Importantly, the largest increase in performance occurs in model C, which incorporates markers of outcome within molecular subtypes.

Improved Risk Stratification Using Molecular Markers

Figure 2C shows the breakdown of standard-risk and high-risk test set patients for model C (best-performing model). Fifteen patients categorized as standard-risk by the current clinical schema actually relapsed. Of those, model C correctly predicts that six (true-positive rate, 0.40; 97.5% CI, 0.14 to 0.71; false-positive rate, 0.11; 97.5% CI, 0.025 to 0.28) will relapse. Despite the large CIs, the difference between the clinical schema and model C remained significant using both DeLong et al⁴⁵ (*P* = .04) and Integrated Discriminant Improvement (IDI) criteria⁴⁶ (see Appendix). These preliminary results show potential practical value for identifying standard-risk patients who may benefit from treatment more suitable for high-risk patients.

DISCUSSION

Our model is one of the first medulloblastoma risk models that maintains good performance on an independent multi-institutional test set, suggesting its generalizability for use in future medulloblastoma clinical trials. Models C and D appear to outperform other state-of-the-art models reported in the literature, such as those of Pfister et al¹⁴ and de Haas et al.¹³ The similarity of our training and test results indicates that our strategy of selecting high-level features and our

model architecture control for overtraining. The significant improvement of model C over the current clinical schema and model A (based on clinical features) and our previously published eight-gene outcome signature can be attributed to the use of highly informative expression signatures, specifically those conditional on disease subtype. Models that do not take into account disease subtype (eg, model B) are inherently less accurate. The use of disease subtype-specific features effectively addresses this problem.

To establish the method's effectiveness on independently acquired data and other acquisition platforms, we applied a simple normalization procedure based on a 0-to-1/min-max rescaling of the expression signatures' activation scores (see Appendix). For eventual clinical deployment, in which a single patient sample must be evaluated, a central laboratory and single platform would eliminate this step, subject to final validation of the model.

Three genomic abnormalities were associated with medulloblastoma outcome in past studies: *c-Myc* and *N-Myc* amplification and monosomy 6 correlate with relapse status but have low penetrance in our training set (8%, 36%, and 16%, respectively). This low penetrance combined with the asymmetry of their corresponding nomogram arms in Figure 3 (indicating low predictive value when absent) limits their value as overall predictors of outcome. In contrast, the overexpression of the *c-Myc* expression signature (third row of Fig 4A) is a significant predictor of relapse with higher penetrance (43%) and has higher predictive value when absent, making it a better predictor of relapse. Our results suggest that in medulloblastomas, multiple mechanisms of *Myc* activation might be at play and would show the advantage of considering catch-all functional readouts of oncogene activation rather than relying solely on the status of known genomic abnormalities. The relevance of *c-Myc* activation as a marker of poor outcome in our study is consistent with its previously implicated role as a significant risk factor^{12,13,42} and a general regulator of poor-prognosis metastatic state.²³

We found that the addition of genomic amplifications and deletions (model D) does not improve accuracy, possibly because we had such data for only about 40% of training and test samples or that the information these loci carry is already subsumed in the expression signatures. For example, the expression of the β -catenin pathway, one of our disease subtype signatures, follows closely the status of del(6q).

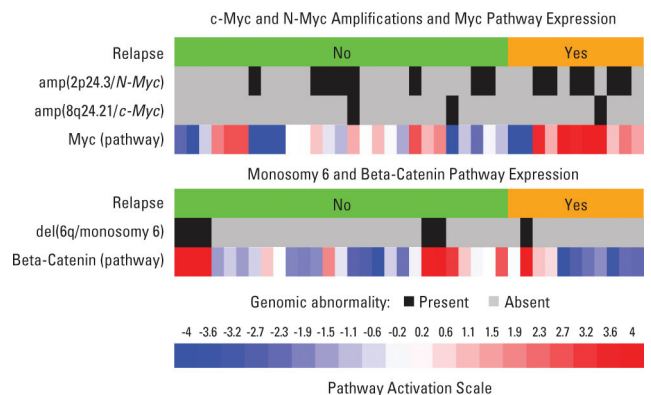


Fig 4. Heat map of 38 samples showing the Genomic Identification of Significant Targets in Cancer (GISTIC) amp(8q24.21/*c-Myc*) status, the GISTIC amp(2p24.3/*N-Myc*) status, the expression of the disease-independent *c-Myc* pathway, the del(6q/monosomy 6) GISTIC status, and the expression of the beta-catenin pathway.

Unfortunately, we have too few samples with copy-number data to address this issue conclusively. Moreover, there were insufficient copy-number data within each subtype to evaluate whether subtype-dependent amplification or deletion has higher predictive value.

One of the four amplifications and deletions we identified as associated with outcome, amp(3q26.32/p110a/PI3K locus) has been associated with poor outcome in endometrial cancer.⁴⁷ A detailed biologic interpretation of the disease subtype-dependent pathways will require a follow-up study. In particular, the *mTOR* pathway, highly upregulated in the disease subtype c_1 , is a central integrator of signals and *AKT* phosphorylation and has been demonstrated to be involved in medulloblastoma.⁴⁸

We introduced a Bayesian nomogram similar to those based on regression models^{49,50} but containing additional elements to represent disease subtype-dependent pathways. For example, the patient shown in Figure 3 has the standard-risk profile, and the current clinical schema incorrectly predicts no relapse. In contrast, models C and D correctly predict relapse because of the cumulative log-odds evidence derived from the genomic features, including *c-Myc* activation. This nomogram shows only the relevant disease subtype (c_1) arms; the full nomogram including all the disease subtype-dependent arms is shown in the Data Supplement.

In summary, we developed a model that predicts relapse in medulloblastoma, retaining high accuracy when applied to an independent multi-institutional validation test cohort. A key feature of the model is the combination of clinical parameters with molecular markers representing gene-expression signatures of mechanisms and pathways that are specific to disease subtypes. The model relies on variable relapse-associated levels of expression signatures within disease subtypes. Considered from the perspective of individual tumor samples, the model allows for outcome predictions along with a measure of the contribution of each individual risk factor. This goes well beyond methods that simply establish association of marker expression levels with disease outcome and gives a clear sense of the possible value of the method in a clinical setting. For example, the model correctly reclassified six of 15 patients who were standard-risk by clinical criteria as high-risk. These six patients represent > 10% of the standard-risk patients in our validation cohort who, up-front, should have been offered more aggressive therapy and a better chance of

progression-free survival than what stratification based on clinical criteria offered.

The model described here represents a first step in obtaining a more accurate, quantitative risk stratification for medulloblastoma patients by taking advantage of multiple sources of information: clinical, molecular, and genetic. While not yet ready for clinical use, with further refinement it might lead to a real-time Clinical Laboratory Improvement Amendments (CLIA)–certified test that clinicians can use to help guide their treatment decisions (see Appendix). Precedent has already been established in breast cancer risk stratification by the *Oncotype DX*⁵¹ and *MammaPrint*⁵² tests currently in prospective clinical trials. Breast cancer has heterogeneity similar to that of medulloblastomas and thus serves as a good metric. These tests have shown that a gene expression–based assay can be performed with rapid turnaround and high sensitivity/specificity. Thus efforts to refine, transfer, and apply our proposed model to medulloblastomas should be a priority.

AUTHORS' DISCLOSURES OF POTENTIAL CONFLICTS OF INTEREST

The author(s) indicated no potential conflicts of interest.

AUTHOR CONTRIBUTIONS

Conception and design: Pablo Tamayo, Yoon-Jae Cho, Scott L. Pomeroy, Jill P. Mesirov

Financial support: Scott L. Pomeroy, Jill P. Mesirov

Provision of study materials or patients: Yoon-Jae Cho, Heidi Greulich, Lauren Ambrogio, Netteke Schouten-van Meeteren, Tianni Zhou, Allen Buxton, Marcel Kool, Matthew Meyerson, Scott L. Pomeroy

Collection and assembly of data: Yoon-Jae Cho, Heidi Greulich, Lauren Ambrogio, Netteke Schouten-van Meeteren, Tianni Zhou, Allen Buxton, Marcel Kool, Matthew Meyerson, Scott L. Pomeroy

Data analysis and interpretation: Pablo Tamayo, Yoon-Jae Cho, Aviad Tsherniak, Scott L. Pomeroy, Jill P. Mesirov

Manuscript writing: Pablo Tamayo, Yoon-Jae Cho, Aviad Tsherniak, Heidi Greulich, Lauren Ambrogio, Netteke Schouten-van Meeteren, Tianni Zhou, Allen Buxton, Marcel Kool, Matthew Meyerson, Scott L. Pomeroy, Jill P. Mesirov

Final approval of manuscript: Pablo Tamayo, Yoon-Jae Cho, Aviad Tsherniak, Heidi Greulich, Lauren Ambrogio, Netteke Schouten-van Meeteren, Tianni Zhou, Allen Buxton, Marcel Kool, Matthew Meyerson, Scott L. Pomeroy, Jill P. Mesirov

REFERENCES

1. Cho YJ, Pomeroy SL: Targeted therapy in medulloblastoma, in Houghton PJ, Arceci R (eds): *Molecularly Targeted Therapy for Childhood Cancer*. New York, NY, Springer Verlag, 2009, pp 350
2. Packer RJ, Goldwein J, Nicholson HS, et al: Treatment of children with medulloblastomas with reduced-dose craniospinal radiation therapy and adjuvant chemotherapy: A Children's Cancer Group Study. *J Clin Oncol* 17:2127-2136, 1999
3. Albright AL, Wisoff JH, Zeltzer PM, et al: Effects of medulloblastoma resections on outcome in children: A report from the Children's Cancer Group. *Neurosurgery* 38:265-271, 1996
4. Thomas PR, Deutsch M, Kepner JL, et al: Low-stage medulloblastoma: Final analysis of trial comparing standard-dose with reduced-dose neuraxis irradiation. *J Clin Oncol* 18:3004-3011, 2000
5. Bailey CC, Gnekow A, Wellek S, et al: Prospective randomised trial of chemotherapy given before radiotherapy in childhood medulloblastoma: International Society of Paediatric Oncology (SIOP) and the (German) Society of Paediatric Oncology (GPO)—SIOP II. *Med Pediatr Oncol* 25:166-178, 1995
6. Pomeroy SL, Tamayo P, Gaasenbeek M, et al: Prediction of central nervous system embryonal tumour outcome based on gene expression. *Nature* 415:436-442, 2002
7. Crawford JR, MacDonald TJ, Packer RJ: Medulloblastoma in childhood: New biological advances. *Lancet Neurol* 6:1073-1085, 2007
8. Giangaspero R, Perry R, Kelly P, et al: Tumours of the central nervous system, in Kleihues P, Cavenee W (eds): *World Health Organization Classification of Tumours: Pathology and Genetics—Tumours of the Nervous System*. Lyon, France, IARC Press, 2000
9. Eberhart CG, Kepner JL, Goldthwaite PT, et al: Histopathologic grading of medulloblastomas: A Pediatric Oncology Group study. *Cancer* 94:552-560, 2002
10. Gilbertson R, Wickramasinghe C, Hernan R, et al: Clinical and molecular stratification of disease risk in medulloblastoma. *Br J Cancer* 85:705-712, 2001
11. Rutkowski S, von Bueren A, von Hoff K, et al: Prognostic relevance of clinical and biological risk factors in childhood medulloblastoma: Results of patients treated in the prospective multicenter trial HIT'91. *Clin Cancer Res* 13:2651-2657, 2007
12. Lamont JM, McManamy CS, Pearson AD, et al: Combined histopathological and molecular cytogenetic stratification of medulloblastoma patients. *Clin Cancer Res* 10:5482-5493, 2004

13. de Haas T, Hasselt N, Troost D, et al: Molecular risk stratification of medulloblastoma patients based on immunohistochemical analysis of MYC, LDHB, and CCNB1 expression. *Clin Cancer Res* 14:4154-4160, 2008
14. Pfister S, Remke M, Benner A, et al: Outcome prediction in pediatric medulloblastoma based on DNA copy-number aberrations of chromosomes 6q and 17q and the MYC and MYCN loci. *J Clin Oncol* 27:1627-1636, 2009
15. Mendrzyk F, Radlwimmer B, Joos S, et al: Genomic and protein expression profiling identifies CDK6 as novel independent prognostic marker in medulloblastoma. *J Clin Oncol* 23:8853-8862, 2005
16. Haberler C, Slavo I, Czech T, et al: Histopathological prognostic factors in medulloblastoma: High expression of survivin is related to unfavourable outcome. *Eur J Cancer* 42:2996-3003, 2006
17. Thompson MC, Fuller C, Hogg TL, et al: Genomics identifies medulloblastoma subgroups that are enriched for specific genetic alterations. *J Clin Oncol* 24:1924-1931, 2006
18. Fattet S, Haberler C, Legoux P, et al: Beta-catenin status in paediatric medulloblastomas: Correlation of immunohistochemical expression with mutational status, genetic profiles, and clinical characteristics. *J Pathol* 218:86-94, 2009
19. Segal RA, Goumnerova LC, Kwon YK, et al: Expression of the neurotrophin receptor TrkC is linked to a favorable outcome in medulloblastoma. *Proc Natl Acad Sci U S A* 91:12867-12871, 1994
20. Mootha VK, Lindgren CM, Eriksson KF, et al: PGC-1alpha-responsive genes involved in oxidative phosphorylation are coordinately downregulated in human diabetes. *Nat Genet* 34:267-273, 2003
21. Subramanian A, Tamayo P, Mootha VK, et al: Gene set enrichment analysis: A knowledge-based approach for interpreting genome-wide expression profiles. *Proc Natl Acad Sci U S A* 102:15545-15550, 2005
22. Barbie DA, Tamayo P, Boehm JS, et al: Systematic RNA interference reveals that oncogenic KRAS-driven cancers require TBK1. *Nature* 462:108-112, 2009
23. Wolfer A, Wittner BS, Irimia D, et al: MYC regulation of a "poor-prognosis" metastatic cancer cell state. *Proc Natl Acad Sci U S A* 107:3698-3703, 2010
24. Bild AH, Yao G, Chang JT, et al: Oncogenic pathway signatures in human cancers as a guide to targeted therapies. *Nature* 439:353-357, 2006
25. Edelman E, Porrello A, Guinney J, et al: Analysis of sample set enrichment scores: Assaying the enrichment of sets of genes for individual samples in genome-wide expression profiles. *Bioinformatics* 22:e108-e116, 2006
26. Lee E, Chuang HY, Kim JW, et al: Inferring pathway activity toward precise disease classification. *PLoS Comput Biol* 4:e1000217, 2008
27. Burnside ES, Rubin DL, Fine JP, et al: Bayesian network to predict breast cancer risk of mammographic microcalcifications and reduce number of benign biopsy results: Initial experience. *Radiology* 240:666-673, 2006
28. Gevaert O, De Smet F, Timmerman D, et al: Predicting the prognosis of breast cancer by integrating clinical and microarray data with Bayesian networks. *Bioinformatics* 22:e184-e190, 2006
29. Nagl S, Williams M, Williamson J: Objective Bayesian nets for systems modelling and prognosis in breast cancer, in Holmes DE, Jain LC (eds): *Innovations in Bayesian Networks: Theories and Applications*. Berlin, Germany, Springer, 2008, pp 131-167
30. Sebastiani P, Nolan VG, Baldwin CT, et al: A network model to predict the risk of death in sickle cell disease. *Blood* 110:2727-2735, 2007
31. Swartz RJ, West LA, Boiko I, et al: Classification using the cumulative log-odds in the quantitative pathologic diagnosis of adenocarcinoma of the cervix. *Gynecol Oncol* 99:S24-S31, 2005 (suppl 1)
32. Možina M, Demšar J, Kattan M, et al: Nomograms for visualization of naive Bayesian classifier. Presented at the 8th European Conference on Principles and Practice of Knowledge Discovery in Databases, Pisa, Italy, September 20-24, 2004
33. Kool M, Koster J, Bunt J, et al: Integrated genomics identifies five medulloblastoma subtypes with distinct genetic profiles, pathway signatures and clinicopathological features. *PLoS One* 3:e3088, 2008
34. Yu D, Cozma D, Park A, et al: Functional validation of genes implicated in lymphomagenesis: An in vivo selection assay using a Myc-induced B-cell tumor. *Ann N Y Acad Sci* 1059:145-159, 2005
35. Majumder PK, Febbo PG, Bikoff R, et al: mTOR inhibition reverses Akt-dependent prostate intraepithelial neoplasia through regulation of apoptotic and HIF-1-dependent pathways. *Nat Med* 10:594-601, 2004
36. Högerkorp CM, Bilke S, Breslin T, et al: CD44-stimulated human B cells express transcripts specifically involved in immunomodulation and inflammation as analyzed by DNA microarrays. *Blood* 101:2307-2313, 2003
37. Collier HA, Grandori C, Tamayo P, et al: Expression analysis with oligonucleotide microarrays reveals that MYC regulates genes involved in growth, cell cycle, signaling, and adhesion. *Proc Natl Acad Sci U S A* 97:3260-3265, 2000
38. Kegg: Histidine metabolism: Reference pathway. <http://www.genome.jp/kegg/pathway/map/map00340.html>
39. Yoon JW, Kita Y, Frank DJ, et al: Gene expression profiling leads to identification of GLI1-binding elements in target genes and a role for multiple downstream pathways in GLI1-induced cell transformation. *J Biol Chem* 277:5548-5555, 2002
40. Zhang Y, Jamaluddin M, Wang S, et al: Ribavirin treatment up-regulates antiviral gene expression via the interferon-stimulated response element in respiratory syncytial virus-infected epithelial cells. *J Virol* 77:5933-5947, 2003
41. Cho J-Y, Tsherniak A, Tamayo P, et al: Integrative genomic analysis of medulloblastoma identifies a molecular subgroup that drives poor clinical outcome. *J Clin Oncol* 29:1424-1430, 2011
42. Herms J, Neidt I, Lüscher B, et al: C-MYC expression in medulloblastoma and its prognostic value. *Int J Cancer* 89:395-402, 2000
43. Beroukhi R, Getz G, Nghiemphu L, et al: Assessing the significance of chromosomal aberrations in cancer: Methodology and application to glioma. *Proc Natl Acad Sci U S A* 104:20007-20012, 2007
44. Baker SG, Cook NR, Vickers A, et al: Using relative utility curves to evaluate risk prediction. *J R Stat Soc Ser A Stat Soc* 172:729-748, 2009
45. DeLong ER, DeLong DM, Clarke-Pearson DL: Comparing the areas under two or more correlated receiver operating characteristic curves: A nonparametric approach. *Biometrics* 44:837-845, 1988
46. Pencina MJ, D'Agostino RB Sr, D'Agostino RB Jr, et al: Evaluating the added predictive ability of a new marker: From area under the ROC curve to reclassification and beyond. *Stat Med* 27:157-172, 2008; discussion 207-212
47. Salvesen HB, Carter SL, Mannelqvist M, et al: Integrated genomic profiling of endometrial carcinoma associates aggressive tumors with indicators of PI3 kinase activation. *Proc Natl Acad Sci U S A* 106:4834-4839, 2009
48. Dickson BC, Mulligan AM, Zhang H, et al: High-level JAG1 mRNA and protein predict poor outcome in breast cancer. *Mod Pathol* 20:685-693, 2007
49. Harrell FE: *Regression Modeling Strategies: With Applications to Linear Models, Logistic Regression, and Survival Analysis*. New York, NY, Springer-Verlag, 2001
50. Iasonos A, Schrag D, Raj GV, et al: How to build and interpret a nomogram for cancer prognosis. *J Clin Oncol* 26:1364-1370, 2008
51. Cronin M, Sangli C, Liu ML, et al: Analytical validation of the Oncotype DX genomic diagnostic test for recurrence prognosis and therapeutic response prediction in node-negative, estrogen receptor-positive breast cancer. *Clin Chem* 53:1084-1091, 2007
52. Slodkowska EA, Ross JS: MammaPrint 70-gene signature: Another milestone in personalized medical care for breast cancer patients. *Expert Rev Mol Diagn* 9:417-422, 2009

